NO_3 radical studied by laser-induced fluorescence

Bongsoo Kim, Philip L. Hunter, and H. S. Johnston
Department of Chemistry, University of California, and Chemical Sciences Division, Lawrence Berkeley Laboratory, Berkeley, California 94720

(Received 11 June 1991; accepted 28 October 1991)

The fluorescence emission spectra of NO_3 excited at 14 742, 15 109, 15 882, 16 053, and 16 555 cm^{-1} are reported. On the basis of fundamentals, overtones, and combination of five vibrational frequencies (368, 753, 1053, 1500, and 2010 cm^{-1}) we assign 18 out of 20 observed bands. The fluorescence bands exhibit two different shapes, one shows a sharp spike overlapped with a broadband, and the other shows a broadband only. From the literature we obtain a potential-energy surface that has D_{3h} symmetry with three identical shallow minima, each representative of a local C_{2v} structure and located with threefold symmetry around the central axis. Such a potential-energy function can split degenerate D_{3h} vibrational modes, giving "pseudorotations," as a structure with one long and two short bonds permutes around the three minima. On the time scale of molecular rotations, vibrational motions average over the three local C_{2v} structures to give D_{3h} structure and rotational spectra. This model qualitatively explains both the five fundamental frequencies observed by fluorescence and the definite D_{3h} properties of high-resolution infrared spectra. We suggest that a molecular theoretical model with fine spatial resolution sees the miniwells and reports C_{2v} as minimum-energy structure, but a model with less fine resolution overlooks the three shallow minima and reports the larger-scale D_{3h} structure.

I. INTRODUCTION

Ramsay[1] and Marinelli, Swanson, and Johnston[2] observed the absorption spectrum of NO_3 at high resolution, and both reported that all the NO_3 bands are diffuse. They ascribed the diffuseness to extensive vibronic perturbation (Douglas coupling).[3] In 1983 Ishiwata *et al.*[4] reported dispersed laser-induced fluorescence of NO_3, which showed bands at 380, 1060, 1490, and 760 cm^{-1} when excited by a 661.8 nm laser. Their spectral resolution was about 40 cm^{-1} at 700 nm. They suggested D_{3h} symmetry for ground-state NO_3 and assigned fundamental frequencies as to 380 (ν_4,e'), 1060 (ν_1,a_1'), and 1480 cm^{-1} (ν_3, e'). Nelson, Pasternach, and McDonald[5] reported a similar laser-induced fluorescence spectrum with slightly better resolution, 35 cm^{-1} at 700 nm. On the basis of C_{2v} geometry, they assigned fundamental frequencies as 1051 (a_1), 754 (a_1), 1489 (b_2), and 360 (b_2) cm^{-1}. They observed but did not assign frequencies at 1910, 2000, and 2336 cm^{-1}.

In 1985 Ishiwata *et al.*[6] reported the infrared spectrum of NO_3 in the 1492 cm^{-1} region using a Zeeman modulation diode laser spectrometer. The analysis of the IR spectrum requires D_{3h} symmetry, since only $K'' = 3n$ (n = integer) transitions were observed. They found several anomalous features. Friedl and Sander[7] observed three vibrational bands of NO_3 in 759.6, 762, and 1492 cm^{-1} using Fourier-transform infrared spectroscopy with 0.005 cm^{-1} resolution. The IR spectra at 762 and 1492 cm^{-1} showed D_{3h} symmetry. The band centered at 759.6 cm^{-1} showed features characteristic of a parallel band but resisted any simple assignment. They suggested the possible existence of a low-lying electronic state approximately 100 cm^{-1} above the ground state.

Kawaguchi *et al.*[8] reinvestigated the NO_3 1492 cm^{-1} band, and they were able to remove all of the anomalies for the ground state in the previous assignment.[6] The spin–orbit interaction constant for the upper state at 1490 cm^{-1} above the ground state was unusually small compared with other cases.

Weaver *et al.*[9] observed ultraviolet photoelectron spectra of the nitrate anion, which showed the transition to $^2A_2'$ and $^2E''$ electronic states of NO_3. In the transition to $^2A_2'$ they observed about 12 vibrational peaks and assigned the five most intense peaks as the vibrational progressions of 1080 cm^{-1} (ν_1,a_1') and 363 cm^{-1} (ν_4, e'). The instrumental resolution for their experiment was 64 cm^{-1}. Anomalies in the intensities and the peak positions of the vibrational progressions were seen and explained as pseudo–Jahn–Teller coupling between the $^2A_2'$ and $^2E'$ states of NO_3. They reported that the coupling strength necessary to reproduce their results did not break the D_{3h} symmetry of the $^2A_2'$ state.

In parallel with the experimental work, there are many theoretical calculations[10–18] studying the ground state NO_3. Using unrestricted–Hartree–Fock (UHF) wave functions, Lund and Thuomas[10] found that the ground state of NO_3 possessed D_{3h} symmetry with an N–O bond length of 0.124 nm. Siegbahn[11] tried geometry optimization on NO_3 using complete-active-space self-consistent-field (CASSCF) and configuration-interaction (CI) wave functions, restricted optimization to planar geometries, and kept the three N–O bond lengths the same to explore around D_{3h} geometry. In his calculation the restricted optimization did not converge to D_{3h} geometry. Kaldor[12] used the coupled cluster single and double (CCSD) method, found D_{3h} symmetry, and evaluated frequencies at the optimized D_{3h} geometry.

Boehm and Lohr[13] reported theoretical results for sev-

 0021-9606/92/064057-11$06.00

eral electronic states of NO_3. They used UHF wave functions and applied Møller–Plesset perturbation. Their optimized geometry of the NO_3 ground state depended on the level of perturbation theory. Davy and Schaefer[14] used the high-level CASSCF calculation, employing more than 100 000 configuration state functions. They found minimum energy for C_{2v} geometry. The energy of this C_{2v} minimum geometry is 1.4 kcal/mol (490 cm^{-1}) below that of the D_{3h} minimum geometry. Some vibrational frequencies obtained at the D_{3h} minimum geometry showed large deviation from the experimental frequencies.

Using multiconfiguration SCF (MCSCF) wave functions, Kim *et al.*[15] obtained minimum energy with a C_{2v} structure and calculated vibrational frequencies at that geometry. Similar results were obtained in the vibrational frequency analyses by Davy[16] and Morris, Bhatia, and Hall.[17]

This experimental study extends the work of Refs. 4 and 5, and we obtain laser-induced fluorescence (LIF) spectra of NO_3 for several excitation frequencies. Our highest resolution is 2.5 cm^{-1}, most studies are at 4 cm^{-1} resolution, which is about 8 times higher than that of the previous fluorescence studies,[4,5] and we find additional vibrational bands in a region that was not covered before.

Kawaguchi *et al.*[8] wrote, "It is still quite difficult to conceive and prove a particular model for the NO_3 radical that is compatible with all the experimental evidences." However, they suggested a plausible model for NO_3 for which one of the N–O bonds is longer than the other two bonds of equal length, with a low barrier between the three equivalent C_{2v} minima. Stanton, Gauss, and Bartlett[18] developed this idea, finding the C_{2v} minima to be about 900 cm^{-1} below the D_{3h} second-order saddle point, and the barrier between the C_{2v} minima to be about 192 cm^{-1}. With such a potential-energy surface, NO_3 would have an almost free "pseudorotation about the D_{3h} stationary point, along a pathway which contains three minima [one long and two short bonds] and three transition states [two long and one short bonds]." Figure 1 presents this concept, which is adapted from a figure given by Morse *et al.*[19] They carried out a complete analysis of the spectrum of the trimer of copper, fitted a potential surface to the data, and solved Schrödinger's equation for the overall D_{3h} potential-energy surface with three shallow C_{2v} minima. The overall potential-energy surface has D_{3h} symmetry, but each of the three structures of lowest potential energy is C_{2v}.[19] Table I summarizes recent theoretical calculations and includes both "C_{2v}" and "D_{3h}" observed vibrational frequencies, based on literature references and on values we found in this study. Table I also presents observed[20–22] frequencies for FNO_2. In this article we use the qualitative concepts of Fig. 1 and the entries of Table I in discussing our experimental results.

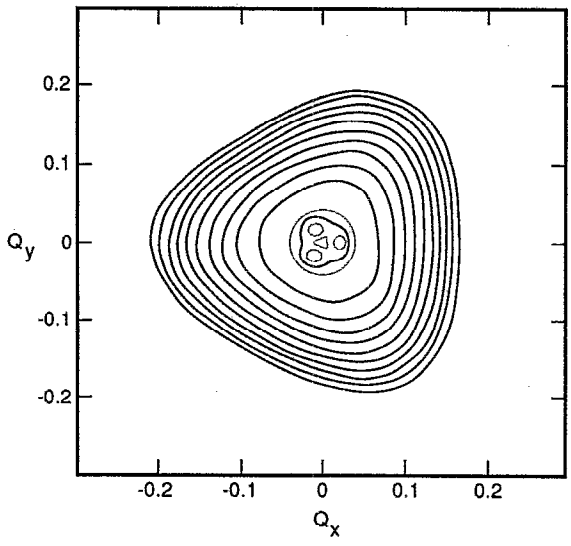

FIG. 1. Contour diagram of the lower component of the $^2E''$ potential-energy surface proposed as explanation of spectral features of Cu_3, adapted from Ref. 19. In the present article, its features are used to give a qualitative explanation of some spectral features of NO_3. The potential surface has D_{3h} structure, and with threefold symmetry it has three equal minima, each with local C_{2v} structure.

II. EXPERIMENT

Figure 2 is a schematic diagram of the experimental system. We flow a stream of helium through a thermostated sample of anhydrous nitric acid. Another stream of 95% helium and 5% fluorine passes through quartz tubes in a microwave-driven plasma (2450 MHz) to form atomic fluorine. The streams are blended and the fluorine atoms react with nitric acid vapor to produce NO_3:

$$F + HNO_3 = HF + NO_3.$$

We monitor the flow rate of each stream by a Hastings mass flow meter. In the cell we adjust the total pressure (measured by an MKS Baratron capacitance manometer) of the flowing gases between 120 and 600 mTorr. Flow rates and total pressure are adjusted to give an optimum NO_3 fluorescence signal.

We use the Spectra Physics 165-09 argon-ion continuous laser to pump the Spectra Physics 375 standing-wave dye laser. The laser bandwidth is nominally 1 cm^{-1} at 15 109 cm^{-1}. The laser beam, TEM (0,0), is softly focused onto the detection region of the cell, using a 50 cm focal-length lens. With 4.2 W pumping power, the DCM dye delivers 500–700 mW in the 620–680 nm range, and the Rh6G dye gives 300–700 mW of power covering the 580–630 nm range. We use a light stabilization circuit to adjust the argon-ion laser power and to maintain the power stability within $\pm$ 1% during 10 h.

We collect the dispersed fluorescence spectrum by a 14 cm focal length, 12 cm diam plano-convex lens, which is placed 19 cm away from the detection cell and focused over a distance of 75 cm onto the entrance slit of a 1 m Czerny–Turner monochromator (Interactive Technology CT-103). With 33 cm focal-length slit lenses, the monochromator utilizes the full height of the slits (5 cm); it has a grating with 1200 grooves per mm blazed at 500 nm. External optics focuses the dispersed fluorescence onto the cooled photocathode of an RCA 31034A photomultiplier tube (PMT). We calibrate the system response with a broad-strip tungsten lamp and radiant temperature measuring device (Fig. 3).

TABLE I. Fundamental frequencies (cm^{-1}) of NO_3 from *ab initio* calculations and those observed from similar molecules according to D_{3h} and C_{2v} models.

(A) D_{3h} Normal mode	Obs. NO_3^- [a]	Obs. NO_3 [b]	Obs. [c]	*Ab initio* calculated [d]	*Ab initio* calculated [e]
$\nu_1(a_1')$ sym. str.	1050	1060	1053	1133	1068
$\nu_2(a_2'')$ out-of-plane bend	831		753	776	
$\nu_3(e')$ asym. str.	1390	1480	1500	1163	963
$\nu_4(e')$ asym. bend	720	380	368	277	596*i*

(B) C_{2v} Normal mode [f]	For FNO_2	Obs. FNO_2 [g]	Obs. NO_3 [c,h]	*Ab initio* NO_3 [i]	*Ab initio* NO_3 [j]	*Ab initio* NO_3 [h]
$\nu_1(a_1)$	NO sym. stretch	822	1053[f]	1112	1122	1024
$\nu_2(a_1)$	NF stretch	1310	1500[f]	1562	1590	1483
$\nu_3(a_1)$	ONO bend	568	···	738	741	682
$\nu_4(b_1)$	out-of-plane bend	742	753	884	877	801
$\nu_5(b_2)$	asym. stretch	1792	2010	1864	2005	1843
$\nu_6(b_2)$	asym. bend	560	368	595	686	506

[a] G. Herzberg, *Molecular Spectra and Molecular Structure. II. Infrared and Raman Spectra of Polyatomic Molecules* (van Nostrand, New York, 1945), p. 178.
[b] Reference 4.
[c] Values from this work.
[d] Reference 12.
[e] Reference 14, D_{3h} imposed.
[f] Figure 18 for NO_3.
[g] References 20–22.
[h] Reference 17, DZP basis set CISD.
[i] Reference 15, TZP basis set, restricted HF.
[j] Reference 16, DZP basis set, unrestricted HF. In this table and Fig. 18, normal-mode number 1 in C_{2v} is defined as the one that goes over to the nondegenerate stretching mode (a_1') in the limit of D_{3h}.

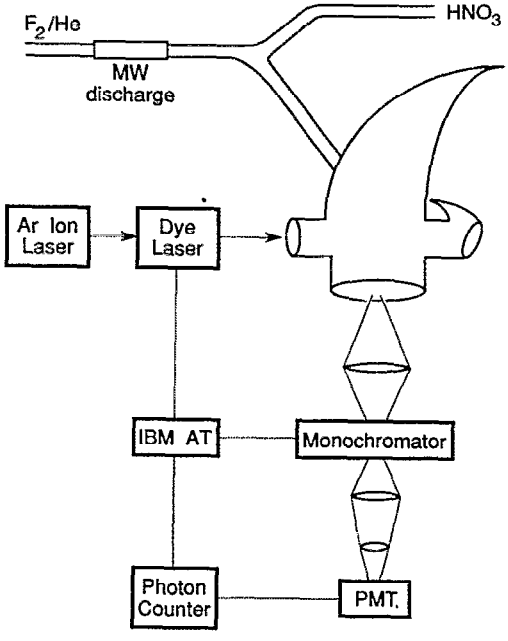

FIG. 2. The experimental setup of the laser-induced fluorescence experiment. An IBM AT computer controls dye laser stepping motor, photon counter, and the monochromator.

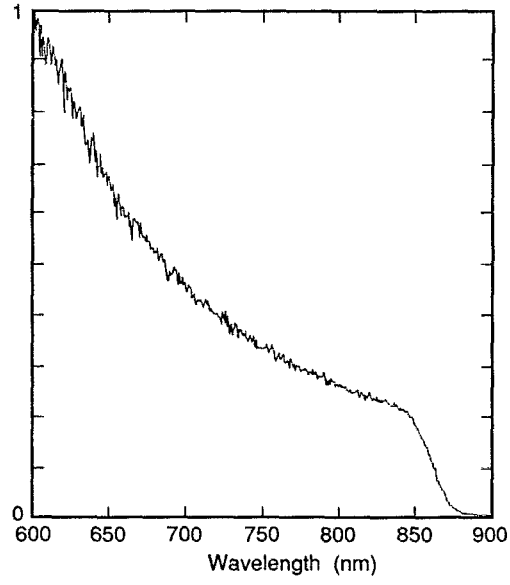

FIG. 3. Relative response of the system to photons of different wavelength from 600 to 900 nm, evaluated by scanning the monochromator while using a special tungsten lamp with measured surface temperature and tabulated emissivity.

We calibrate the monochromator with respect to wavelength by using known emission lines from a low-pressure mercury lamp and a neon pilot lamp. Scattered laser light, processed through the monochromator, gives the wavelength of the dye laser radiation. The monochromator slits are typically set at 250 μm, which give a bandpass of 0.2 nm [full width at half maximum (FWHM)] and 4 cm^{-1} resolution at 700 nm. Some of the spectra are taken with the slit width of 150 μm, giving the resolution of 2.5 cm^{-1} at 700 nm. A computer-controlled stepping motor scans the monochromator.

All of the spectra reported here were obtained by photon counting. We send the output from the fluorescence collection PMT to a PAR 1121 high gain amplifier/discriminator, which is interfaced to a homemade pulse counter card and a microcomputer (IBM AT). Dry ice maintains the photomultiplier at -45 °C, and the dark count is less than 2 counts per second when the PMT bias voltage is -1650 V.

Using an IBM AT computer and stepping motor to drive the intracavity birefringent filter, we scan the laser wavelength to obtain the excitation spectrum, which is recorded by collecting the fluorescence dispersed at 662 nm or at 711 nm (depending on the excitation wavelength) with the monochromator slits open to 3 mm.

We prepare anhydrous HNO_3 by distilling a mixture of $NaNO_3$ and concentrated H_2SO_4 at 310 K and collecting HNO_3 at 233 K. During the experiment, anhydrous nitric acid is kept in a saturator at 289 K. The gases used in the experiment were obtained from Lawrence Berkeley Laboratory (He) and Matheson (5% F_2 in He) and used as received.

Fluorescence experiments with nitrogen dioxide established that its fluorescence does not significantly contribute to the spectra reported here.

III. RESULTS

A. 0–0 excitation at 15 109 cm^{-1}

The peak of the absorption band that corresponds to the 0–0 excitation from the ground state to $^2E'$ state occurs at 15 109 cm^{-1} (we retain extra significant figures to support small differences in later discussions). Figure 4 presents the dispersed laser-induced fluorescence (LIF) of NO_3 excited at 15 109 cm^{-1} and corrected for monochromator, photomultiplier tube (PMT), and optics according to Fig. 3. On the right-hand side of Fig. 4, we expand the scale by a factor of 5 to show the shape and peak location of the weak bands. The columns of Table II give (i) the sequence number of the peaks in Fig. 4, (ii) the frequency of each peak, (iii) the frequency difference between 15 109 and the observed peak, (iv) the relative intensity of each peak, (v) a tentative assignment of the peaks using the D_{3h} normal coordinate notation of Table I(A), (vi) the difference between the assigned frequency and column (iii), and (vii) a statement of whether the peak shows a sharp spike. Most of the peaks in the spectrum show a sharp spike on top of the broadband, while some peaks including the one at 368 cm^{-1} from the excitation frequency show a broadband only. In Figs. 5 to 11, we select and expand some bands in Fig. 4 in order to illustrate various aspects of the data.

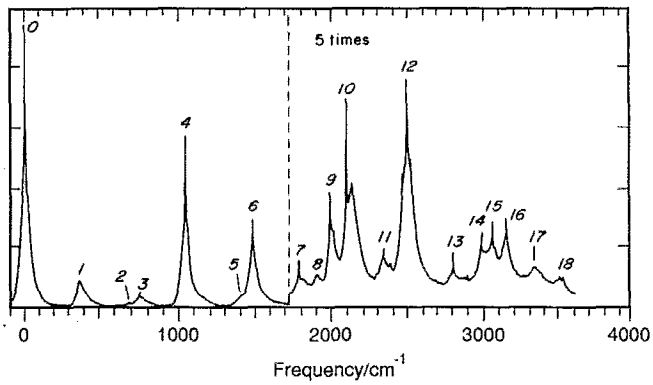

FIG. 4. Dispersed fluorescence with 15 109 cm^{-1} excitation. The x axis is the frequency of the fluorescence subtracted from the excitation frequency. The sharp spike at the excitation frequency is about 50% scattered laser light. The spectrum on the right-hand side of the dotted line is magnified by 5 to show details. The fluorescence was detected to 875 nm over a range of 3600 cm^{-1}.

Following the literature, we assign peak 4 of Fig. 4 at 1053 cm^{-1} as the symmetric stretching normal mode (ν_1), and this is the value entered in Table I. The fluorescence spectrum of this band, obtained with the slit width of 150 μm and resolution of 2.5 cm^{-1}, is given in Fig. 5. There is no resolution of rotational features. The band is surmounted by a spike with full width at half maximum (FWHM) of 4.4 cm^{-1}, and the band itself has FWHM of 63 cm^{-1}. To obtain adequate signal relative to noise, we acquired all other spectra reported here with 250 μm slit (4 cm^{-1} resolution at 700 nm), and a comparison between this higher-resolution profile with the same profile obtained with the usual lower resolution is given by

Resolution	FWHM, band	FWHM, spike	Spike ht./band ht.
2.5 cm^{-1}	63 cm^{-1}	4.4 cm^{-1}	0.82
4.0 cm^{-1}	67 cm^{-1}	5.5 cm^{-1}	0.59

The apparent spike width and relative spike height are distinctly degraded by going from 2.5 to 4.0 cm^{-1} resolution.

The resonance fluorescence, that is, the zero–zero transition, is 64 cm^{-1} FWHM, and it shows a strong spike. In a series of four scans through the 0–0 transition, we found the band to average FWHM of 64 cm^{-1}, the spike to average 5.6 cm^{-1}, and the ratio of spike height/peak height to be 4. These FWHM are about the same as those observed for the ν_1 band in the chart above, but the spike is much higher for the 0–0 band, which is mostly due to scattered laser light. The spectral width of the dye laser is about 1.0 cm^{-1}; within experimental error the apparent FWHM of the scattered light at the resonance band is equal to the FWHM of the spikes observed in these experiments, and thus it is probable that the spike width would be about equal to the laser bandwidth at high resolution.

Some fluorescence bands do not show the sharp spike. The band peaking at 368 cm^{-1} (given in Table I(A) as ν_4, the e' antisymmetric bend) never shows a sharp spike, for

TABLE II. Dispersed fluorescence with 15 109 cm^{-1} excitation (Fig. 4).

Band	ν (cm^{-1})	15 109-ν	Height	Assignment[a]	Diff.[b]	Spike?
0	15 109	0	166	0–0		
1	14 742	368	17	ν_4	[c]	N
2	14 426	693	3	$\nu_1 - \nu_4$	18	Y?[d]
3	14 356	753	11	ν_2	[c]	Y
4	14 056	1053	100	ν_1	[c]	Y
5	13 690	1420	6	$\nu_1 + \nu_4$		?
6	13 609	1500	51	ν_3	[c]	Y
7	13 310	1799	6	$\nu_1 + 2\nu_4$ (or $\nu_1 + \nu_2$)	-10 ($+7$)	Y
8	13 186	1923	4			N
9	13 099	2010	14	A[e]		Y
10A	12 994	2115	24	$2\nu_1$	-9	Y
10B	12 959[f]	2150	15	$\nu_1 + 3\nu_4$	7	N
11	12 751	2358	7	$\nu_4 + A$	0	Y
12	12 598	2511	27	$\nu_1 + \nu_3$	42	Y
13	12 301	2808	6	$2\nu_1 + 2\nu_4$	34	Y
14	12 111	2998	9	$2\nu_3$	2	Y
15	12 406	3063	10	$\nu_1 + A$	0	Y
16	11 953	3156	10	$3\nu_1$	3	Y
17	11 766	3343	5			?
18	11 597	3512	4	$\nu_3 + A$	-2	?
19	11 217	3892	[g]	$3\nu_1 + 2\nu_4$	3	?

[a] See Table I for numbering of D_{3h} modes.
[b] Harmonic position minus observed position in cm^{-1}.
[c] Assigned.
[d] See Fig. 8.
[e] Proposed fifth fundamental frequency.
[f] See Fig. 9.
[g] This is a band observed with the S1 photomultiplier, which has better red sensitivity.

example, Fig. 4 (peak number 1) and Fig. 6. The band shape does not change significantly and the FWHM decreases by 6% as the helium carrier gas pressure changes from 590 to 140 mTorr (Fig. 6 and Table III).

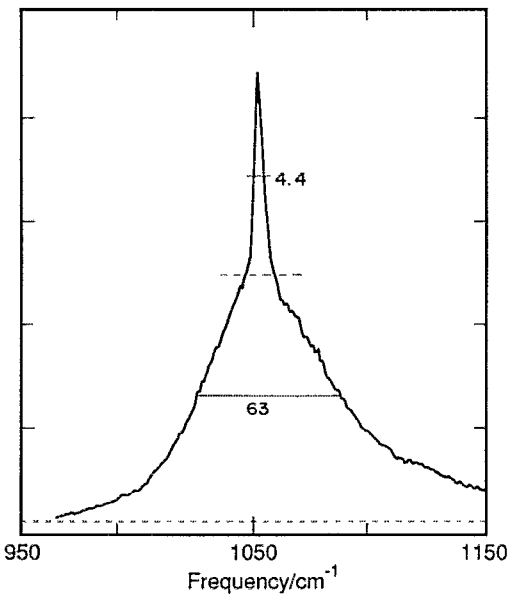

FIG. 5. The fluorescence spectrum obtained with 150 μm slit (2.5 cm^{-1} resolution). ν_{ex} = 15 110 cm^{-1}. Band number 4 on Fig. 2, assigned as ν_1 (see Table I). Note the sharp spike on top of the fluorescence peak. For both the band and the spike, there is a dashed base line; FWHM, solid line.

We set the excitation wavelength at several values between 15 018 and 15 127 cm^{-1} (all inside the envelope of the 0–0 band, which is peaked at 15 109 cm^{-1}) and scanned each fluorescence spectrum. Figures 7–9 give samples of such spectra. In most cases in Fig. 4 (excitation frequency 15 109 cm^{-1}) the spikes are approximately centered on the fluorescence band. In Figs. 7–9 the positions of the broad fluorescence bands do not shift when the excitation frequency is changed, the frequencies of the sharp spikes move along with the change of the excitation frequency, and the differ-

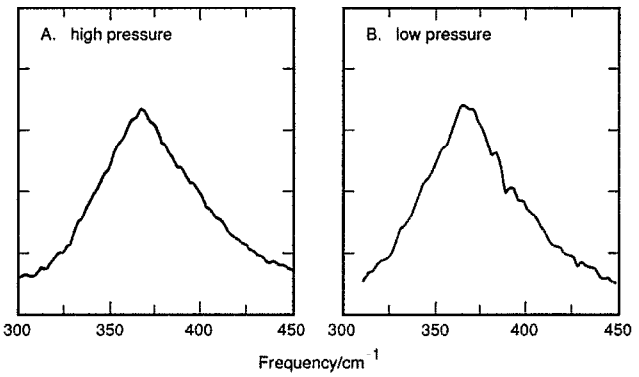

FIG. 6. Band shape and pressure dependence of the fluorescence bandwidth for the 368 cm^{-1} band. Band number 1 in Fig. 2, assigned as ν_4 (see Table I). High pressure 590 mTorr, FWHM, 67 cm^{-1}; low pressure 140 mTorr, FWHM, 63 cm^{-1}.

TABLE III. Ratios of spike and band properties for changes of total pressure (mostly helium carrier gas) for fluorescence bands excited at 15 109 cm^{-1} (compare Figs. 6 and 10). Pressures are in mTorr.

Band center /cm^{-1}	368(ν_4)	1053(ν_1)	1500(ν_2)	2511($\nu_1+\nu_2$)
Pressures (hp/lp)	590/140	590/140	620/140	580/200
Band FWHM (lp)/cm^{-1}	63	58	58	82
Band FWHM (hp/lp)	1.06	1.18	1.05	1.09
Spike FWHM (lp)/cm^{-1}	no spike	5.0	5.6	(8)
Spike FWHM (hp/lp)	no spike	1.14	1.11	1.0
Spike ht./band ht., hp		0.65	0.68	0.37
Spike ht./band ht., lp		1.03	1.00	0.59

ence between excitation frequency and spike frequency remains the same for a given band while both move. The 0–0 fluorescence envelope and scattered light spike do the same. This behavior is observed for all the bands which have a sharp spike, including 19 cases not included in Figs. 7–9.

The shape of the fluorescence bands and the height of the spikes change as the excitation frequency is varied inside the 0–0 absorption band between 15 018 and 15 127 cm^{-1}. Peak 4 at 1053 cm^{-1} (symmetric stretch, ν_1) and peak 6 at 1500 cm^{-1} (degenerate asymmetric stretch, ν_3) show strong centered sharp spikes in Fig. 4, and they show weak off-center sharp spikes in Fig. 7. The FWHM of the ν_1 band changes strongly from 108 to 86 to 70 cm^{-1} as the excitation frequencies go from 15 018 to 15 069 to 15 127 cm^{-1} (Fig. 7), and the width of the ν_3 band undergoes a comparable change. At the two lower excitation frequencies, the spikes are small; that for ν_3 is scarcely greater than the noise. At 15 127 cm^{-1} excitation both spikes are sharp, tall, and off-center (Fig. 7). Figure 8 shows similar effects for peak 3 at 754 cm^{-1}, which we assign as the out-of-plane bend, ν_2, and for the weak combination band (peak 2) at 693 cm^{-1}. The FWHM of ν_2 is almost the same, 72 and 74 cm^{-1}, as the excitation frequency is changed from 15 109 to 15 127 cm^{-1}; but the spike height changes more than a factor of 5 (Fig. 8). The peak at 693 cm^{-1} moves with excitation frequency like the spikes, but the fluorescence is so weak that it is uncertain whether to classify it as having a spike (Note "Y?" in Table II). Figure 9 illustrates these effects for peak 9 at 2010 cm^{-1} (unassigned with D_{3h} modes) and peak 10, which appears to be two overlapping bands, 10*A* and 10*B*. Peaks 9 and 10*A* show strong spikes when excited at 15 111 cm^{-1} (close to the absorption peak at 15 109), weak spikes when excited off-center to the blue at 15 129, and almost no spike when excited off-center to the red at 15 069 (Fig. 9). Peak 10 is exceptionally wide (Table III), which is consistent with its being two overlapping bands. The appearance of Figs. 9(B) and 9(C) suggests that 10 consists of two overlapping bands, 10*A* peaking at 2120 cm^{-1} with a spike and 10*B* peaking at about 2150 cm^{-1} with no spike. Bands 9 and 10 are close together and partially overlapping, so that it is difficult to assign FWHM; however, it appears that the bands excited off-center [Figs. 9(A) and 9(C)] are broader than that excited near the center [Fig. 9(B)].

For the five bands in Figs. 7–9, a spike is sharpest when the excitation is at or near 15 109, the absorption maximum, and the spike height falls off rapidly as the excitation line is shifted either above or below 15 109 cm^{-1}. The main band broadens as the excitation line is set away from 15 109 cm^{-1}, especially toward the red side.

The band profiles and the spike properties change moderately with change in total pressure (mostly helium carrier gas) from 140 to 590 mTorr, as illustrated for ν_3 in Fig. 10. Although there is some uncertainty as to where to draw the base lines, we show base lines for the band and for the spike as dashed lines in the figure. The ratio, spike height/band height, is 0.68 at the higher pressure and 1.00 at the lower pressure. The ratio, (high-pressure FWHM)/(low-pressure FWHM), is 1.11 for the spike and 1.09 for the band. Table III gives these ratios for four bands, and the excitation frequency is 15 109 cm^{-1} in all cases. For the two fundamental frequencies, 1053 and 1500 cm^{-1}, the various ratios are equal within experimental error, but the combination band

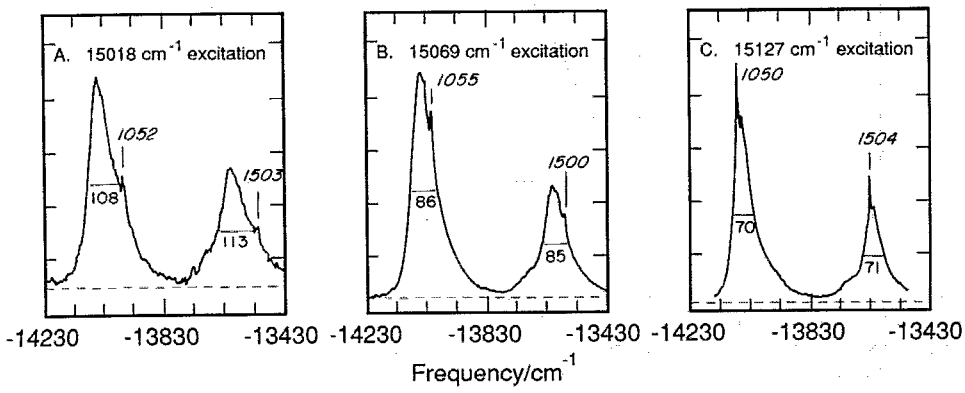

FIG. 7. The frequency of the sharp spikes moves along with the change of excitation frequency, while the broadbands do not move, ν_1 and ν_3, bands 4 and 6 in Fig. 2. The numbers outside the profiles are ν(excitation) − ν(spike). The numbers inside the profiles are FWHM; notice how FWHM and the spike height change strongly with change of excitation frequency inside the absorption band.

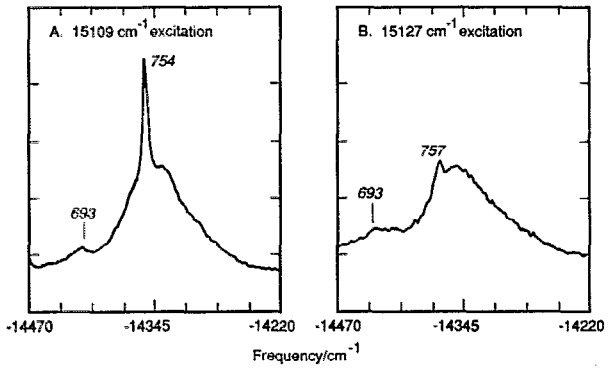

FIG. 8. Same as Fig. 7, except for peak 2 at 693 cm^{-1} and peak 3 at about 754 cm^{-1} (ν_2). The peak of the weak band at 693 cm^{-1} moves in the same way as the spikes, and there may be a weak unresolved spike.

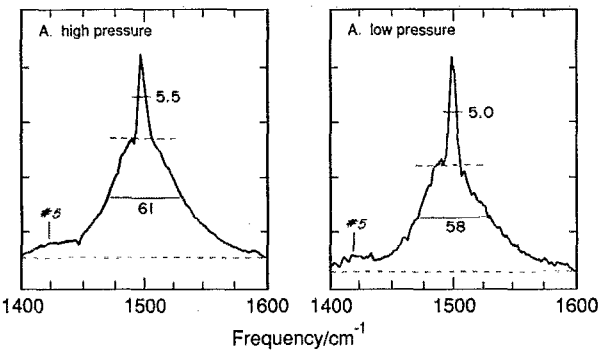

FIG. 10. Band shape and pressure dependence of the fluorescence bandwidth for peak 6 at the 1500 cm^{-1} band. High pressure 620 mTorr, low pressure 140 mTorr. Peak 5 is poorly defined in these figures.

($\nu_1 + \nu_3$) shows substantially lower spike-to-band ratio. The FWHM of this combination band is 1.4 times wider than the other bands in this table, and shoulders were observed inside the band profile. This band may be an overlap of two or more bands.

B. Fluorescence excitation at other than the 0–0 absorption band

Ramsay[1] assigned 944 cm^{-1} as an upper-state frequency, and he observed a progression of overtones of this mode in the absorption spectra. We chose excitation frequencies at the absorption peaks observed in the excitation spectrum by Nelson, Pasternach, and McDonald.[5] In the absorption spectrum of NO_3, there is a weak hot-band peak arising from the excited vibration at 368 cm^{-1}. We measured the dispersed fluorescence spectra excited at four different frequencies ($T+X$) and show them in figures as follows (where $T = 15\,109$ cm^{-1}):

$T + 773 = 15\,882$ (Fig. 11), 629.6 nm;

$T + 944 = 16\,053$ (Fig. 12), 622.9 nm;

$T + 1446 = 16\,555$ (Fig. 13), 604.0 nm;

$T - 368 = 14\,741$ (Fig. 14), 678.4 nm.

The full NO_3 absorption spectrum[23] shows the position of these excitation wavelengths (Fig. 15). In Figs. 11–13, we enter normal-mode symbols above the observed spectrum for peaks that can be interpreted as a direct fluorescence between $T+X$ and a vibrational level of the ground electronic state. Below the observed spectra, we enter normal-mode symbols in square brackets for emissions that can be interpreted as arising from the 15 109 cm^{-1} level and terminating in the ground electronic state. These transitions must have been preceded by collision-induced, vibrational relaxation in the upper electronic state. Peaks that are not marked either way presumably come from partially relaxed vibrational levels in the upper electronic state.

The spectrum excited at $T+773$ (Fig. 11) clearly shows direct fluorescence of ν_4 without a spike. There are spikes corresponding to direct fluorescence from $T+773$ to ground at ν_1 and at ν_3, but there are other, comparably strong, unassigned spikes or noise features in the same region. Fluorescence from the fully vibrationally relaxed upper state to the ground electronic state produces four strong emission bands at [0], [ν_1], [ν_3], and [$2\nu_1$]. The 0–0 transition, which follows collisionally induced relaxation, masks the ν_2 band from the excited level.

In the progression from excitation at T to $T+1446$

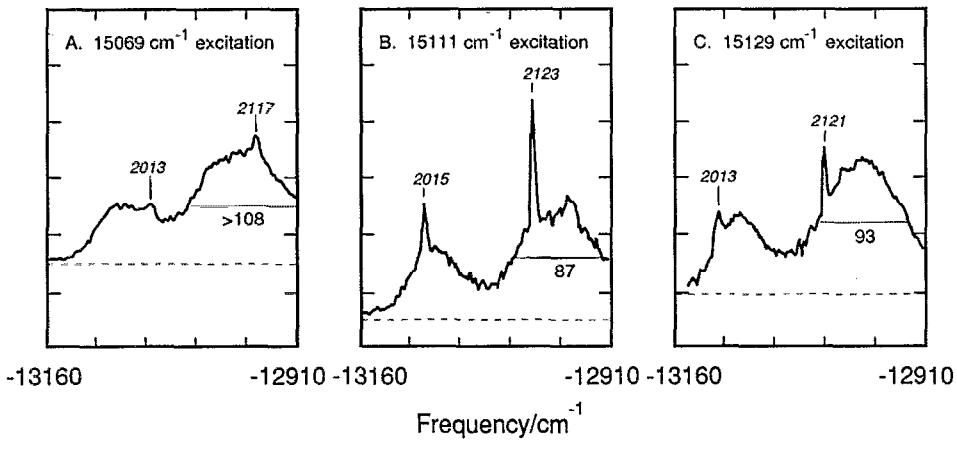

FIG. 9. Same as Fig. 7, except for peak 9 at 2013 cm^{-1} and peak 10, which apparently involves two bands (10*A* and 10*B*). For each of peaks 9 and 10*A*, excitation at 15 069 cm^{-1} gives a weak bump on the red side of of the band center, excitation at 15 129 cm^{-1} gives a distinct spike on the blue side of the band center, and excitation at 15 111 cm^{-1} near the absorption peak gives sharp spikes almost centered on peak 9 but far off center on peak 10. This spike is interpreted as the peak of band 10*A*, and the spike-free band with a maximum at about 2150 is 10*B*.

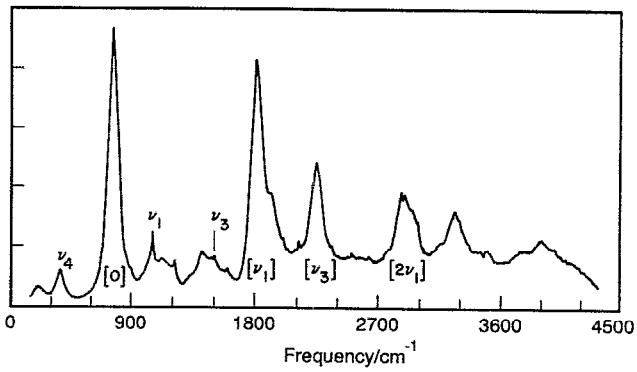

FIG. 11. Dispersed fluorescence with 15 882 cm^{-1} excitation (629.6 nm). This corresponds to 773 cm^{-1} above the 0–0 transition. Vibrational modes indicated above the profiles correspond to fluorescence originating from $T+773$ energy. Vibrational modes indicated below the profiles and contained in square brackets correspond to fluorescence originating from energy $T=15\,109$ cm^{-1}. Both direct fluorescence and fluorescence after vibrational relaxation are seen.

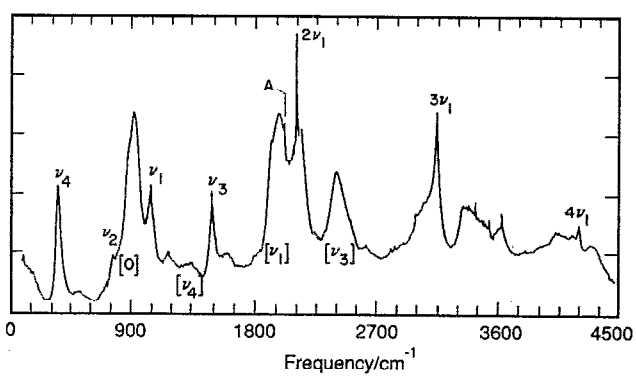

FIG. 12. Similar to Fig. 11, except dispersed fluorescence with 16 053 cm^{-1} excitation, which is 944 cm^{-1} above the 0–0 transition.

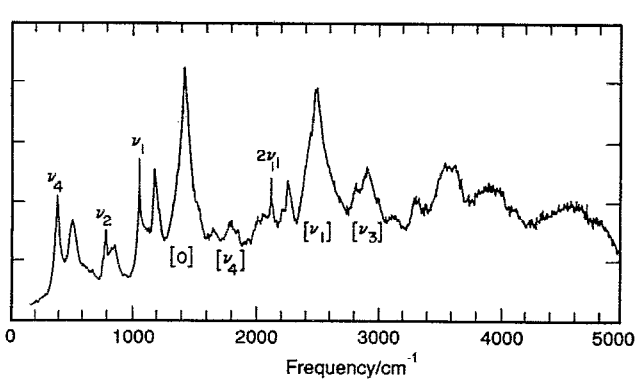

FIG. 13. Similar to Fig. 11, except dispersed fluorescence with 16 555 cm^{-1} excitation, which corresponds to 1446 cm^{-1} above the 0–0 transition.

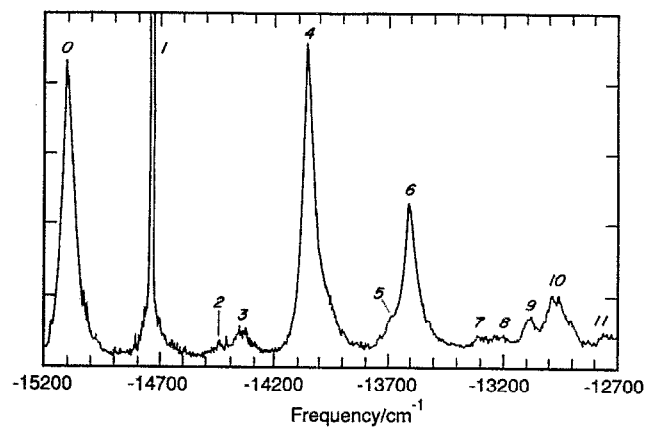

FIG. 14. Dispersed fluorescence with 14 742 cm^{-1} excitation. The hot-band population at 368 cm^{-1} is excited to the $^2E'$ state. The monochromator slits are set at 500 μm. The large spike at the excitation frequency includes scattered laser light. The numbers at the peaks correspond to the sequence numbers of Fig. 4 and Table II.

(Figs. 4, and 11–13), there is a great increase in the unresolved background fluorescence. The spectra of Figs. 11–13 show strong emissions at 15 109 cm^{-1}, which implies collisional deactivation from energy $T+X$ to T in the upper electronic state, followed by $0 \leftarrow T$ emission. Collisional relaxation and the emissions $\nu_1 \leftarrow T$ and $\nu_3 \leftarrow T$ appear in all three figures, and weak $\nu_4 \leftarrow T$ bands may be visible in Figs. 12 and 13. There is direct fluorescence from the excitation energy, $T+X$, to assigned ground-state vibrational levels at ν_1 and ν_4 in three spectra, to ν_3 in two spectra, and to ν_2 (753 cm^{-1} or 775 cm^{-1}) fluorescence in Figs. 12 and 13. Figure 12 shows first, second, and third overtones of ν_1.

The transition frequency from the hot band at 368 cm^{-1} to the upper state at $T=15\,109$ cm^{-1} is 14 742 cm^{-1}, and Fig. 14 gives the fluorescence spectrum excited at this frequency. The peak numbers in Fig. 14 are those of Table II and Fig. 4, and all peaks seen in hot-band excitation (Fig. 14) are included in the 0–0 excitation spectrum (Fig. 4). Figure 16 displays three magnified bands at the 14 742 cm^{-1} excitation. The peaks that showed sharp spikes when excited

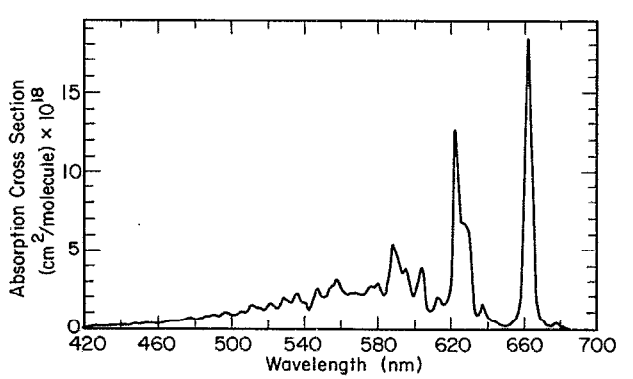

FIG. 15. Absorption spectrum of NO_3 with 1 nm resolution (Ref. 23).

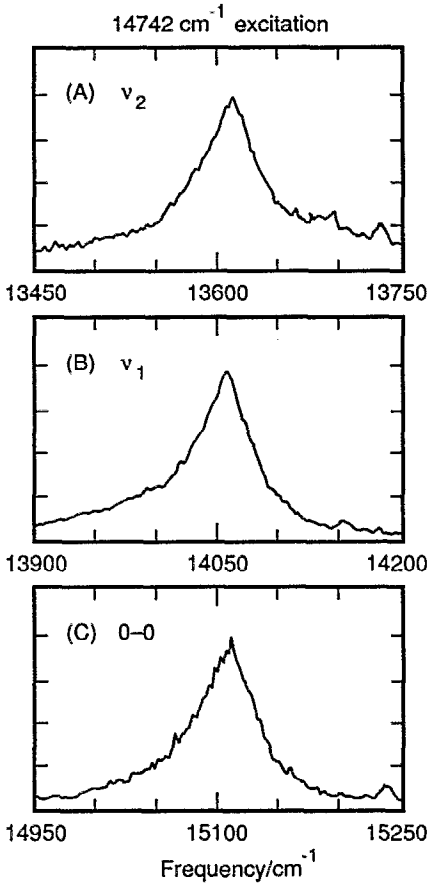

FIG. 16. The magnified band shape of the dispersed fluorescence when excited by 14 742 cm^{-1}, the hot-band excitation. (A) is the band which corresponds to the 1500 cm^{-1} vibrational state, (B) to 1053 cm^{-1}, and (C) to the ground state. No spike is observed.

by 15 109 cm^{-1} do not show spikes with 14 742 cm^{-1} excitation. Since the transition is weak, we set the slit width of the monochromator at 500 μm, which gives about 8 cm^{-1} resolution. With 2.5 cm^{-1} resolution (Fig. 5) the FWHM of the ν_1 spike is 4.4 cm^{-1}. Strong spikes such as that of Fig. 5 could probably be detected with 8 cm^{-1} resolution, but weak spikes, such as those of Figs. 7(A), 7(B), 8(B), 9(A), and 9(C), would probably not been seen.

C. Fluorescence excitation spectra

The fluorescence excitation spectrum obtained by scanning through the 0–0 transition around 15 109 cm^{-1} is shown in Fig. 17(A). The upper half of this profile is almost a triangle, having a sharp top but not a spike. The excitation spectrum around 14 742 cm^{-1}, which is the hot-band excitation from 368 cm^{-1} to 15 109 cm^{-1}, is presented for comparison in Fig. 17(B). The upper half of this profile is almost Gaussian, distinctly broad and rounded relative to the profile of Fig. 17(A).

D. Vibrational analysis in support of interpreting the data

At the time of this experiment there was no theoretical study reported on the vibrational frequencies of NO_3. A vibrational frequency analysis for ground-state NO_3 using *ab initio* methods was performed[15] as an aid in interpreting the experimental data. The geometry optimization resulted in C_{2v} minimum, the vibrational frequencies at that geometry are presented in Table I, and the normal coordinates are given by Fig. 18. In particular, this calculation predicted the asymmetric stretch vibration (b_2) to be 1864 cm^{-1}. Band 1 is assigned to correspond as closely as possible with ν_1 in D_{3h}, not as the highest frequency in a_1.

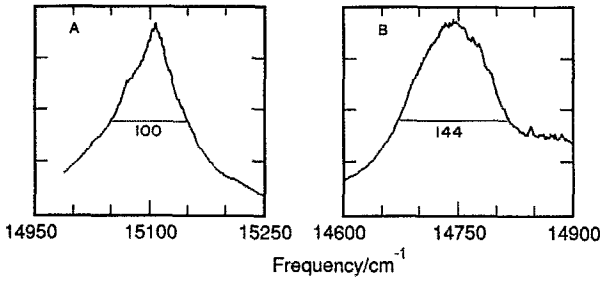

FIG. 17. Magnified NO_3 excitation spectrum around (A) the 0–0 band peaked at 15 109 cm^{-1} and (B) the hot band peaked at 14 742 cm^{-1}.

E. Other patterns in observed fluorescence spectra

When NO_3 is excited to states well above the 0–0 transition to vibronic states at $T+X$, some fluorescence is observed directly from the excited vibronic level down to excited vibrational levels in the ground electronic states. Also, there is strong fluorescence originating at T (15 109 cm^{-1}) and terminating at known vibrational levels in the ground state, suggesting that the rates of vibrational deactivation and fluorescence are comparable in this system. Since rotational relaxation rates are generally faster than vibrational relaxation, it follows that in our system rotational relaxation is much faster than the average rate of fluorescence.

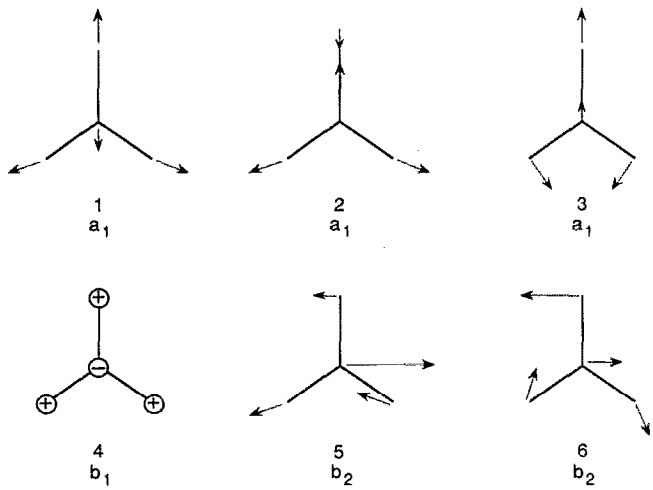

FIG. 18. Normal vibrations of NO_3 for C_{2v} structure, calculated by restricted Hartree–Fock wave functions with triple zeta polarization (TZP) basis set at optimized C_{2v} geometry (Ref. 15). Compare Table I. In the limit of D_{3h} geometry the vibrations ν_2 and ν_5, ν_3 and ν_6 are degenerate.

The mode ν_1 is very nearly harmonic, at least up to the third overtone. In the four dispersed fluorescence spectra (Figs. 4 and 11–13), the first overtone of ν_1 (1053 cm^{-1}) is strongly observed (2115, 2114, 2116, 2119 cm^{-1}) with values close to twice the fundamental (2106), the second overtone is observed (3156, 3154, 3160) at values close to three times the fundamental (3159), and the third overtone observed at 4201 cm^{-1} is close to the harmonic value of 4212. For ν_3 (1500 cm^{-1}) the first overtone is observed (2998, 2998) at values close to the harmonic value of 3000. Higher overtones would be out of the detectable wavelength region of the PMT. The first harmonic overtone of ν_2 (753 cm^{-1}) is 1506, which would be masked by the fundamental at ν_3 (1500), there is no peak near its second overtone at 2259, and no peaks were assigned at any higher overtone. For ν_4 (368 cm^{-1}) there is no fluorescence peak at either its first overtone (736) or at its second overtone (1104). However, ν_4 extensively combines with ν_1 as $\nu_1 + i\nu_4$ where $i = -1$, 1, 2, and 3 (peak numbers 2, 5, 7, and 10*B*, respectively, in Table II) with only a small degree of anharmonicity.

IV. DISCUSSION

A. D_{3h} and C_{2v} symmetry in NO_3 as found by theory

The potential-energy function given by Morse *et al.*[19] for the trimer of copper (Fig. 1) is the qualitative, conceptual basis for discussing the disagreement among various theoretical calculations (Table I). The overall potential-energy surface (PES) has D_{3h} symmetry with three shallow minima, located with threefold symmetry around the central axis. We suggest that a molecular computation with high spatial and energy resolution locates the minimum potential energy at one of the C_{2v} minima, and a method with relatively low resolution averages over the C_{2v} minima to report the minimum as D_{3h}. The standard method of finding normal coordinates locates the global minimum of a multidimensional PES and expands the potential energy in a Taylor series around the minimum. The constant term may be chosen as zero, the linear terms are zero, and quadratic terms are evaluated from the second derivatives or curvatures of the PES at the minimum. Close to the minimum point, third-order and higher terms are negligible. Figure 1 suggests that the curvatures at the bottom of the C_{2v} minima would be different from and probably sharper than the best quadratic approximation of the extended D_{3h} PES. A high-resolution computational method would probably find some sharp curvatures in the C_{2v} minimum, which means large force constants and high calculated frequencies. The three shallow minima circling the D_{3h} axis present a low-resolution method with an apparent flatness, or low curvature, which leads to low force constants and low frequencies. Computations reporting D_{3h} as the structure of lowest energy have symmetric stretch and out-of-plane bending frequencies that agree with experiment, but the two e' frequencies are much lower than observed values (Table I). Models taking one of the C_{2v} structures as the origin, report symmetric stretch and out-of-plane bending frequencies that are about the same as those observed and those calculated by D_{3h}, but the other frequencies are much higher than those calculated by D_{3h}. The remarks agree with the results of Stanton, Gauss, and Bartlett,[18] who found that the barrier between the C_{2v} minima was comparable to the zero-point energy of the lowest observed frequency in NO_3, but it is distinctly lower than the zero-point energies of the observed high frequencies, such as 1053 or 1500 cm^{-1}.

B. D_{3h} and C_{2v} symmetry in NO_3 as indicated by experiment

The infrared studies of Ishiwata *et al.*,[6] Kawaguchi *et al*,[8] and Friedl and Sander[7] require D_{3h} symmetry for infrared absorption bands centered at 762 and 1492 cm^{-1}. In previous fluorescence studies, Ishiwata *et al.*[4] favored D_{3h} symmetry, and Nelson, Pasternach, and McDonald[5] favored C_{2v} symmetry, but these studies did not have data that required either symmetry.

We interpret as many of our peaks as possible using overtones and combinations of the four frequencies (1053, 753, 1500, and 368 cm^{-1}) associated with D_{3h} symmetry. This procedure accounts for the fluorescence spectrum in Fig. 4 except for five peaks, including a strong one at 2010 cm^{-1}. There is a peak (*A*) at 2010 cm^{-1} with high intensity (14% of ν_1), and it appears in three combination bands in the 0–0 excitation spectrum. The closest combination band frequencies to 2010 cm^{-1} are (quantum numbers 0,2,0,1) 1874 cm^{-1} on the lower side and (quantum numbers 2,0,0,0) 2106 cm^{-1} on the upper side, which are outside the range of rotational envelopes. Nelson, Pasternach, and McDonald[5] also observed a strong fluorescence band at 2000 cm^{-1}. By adding 2010 cm^{-1} to the set of four frequencies, we represent all peaks in Fig. 4 as fundamentals, overtones, or combination bands, excepting only the weak peaks at 1923 and 3343 cm^{-1}. On this basis, our data indicate the need for a fifth frequency to represent the fluorescence spectrum, which requires some splitting of the D_{3h} vibrational degeneracy.

C. The nature of the sharp spike

We have considered possible explanations for the observed sharp spikes in the fluorescence spectrum, which move around the emitted band in the same way as the excitation line. Our method uses a laser beam continuous in time. There should be a steady state between formation of electronically excited molecules, rotational and vibrational relaxation of these molecules, and removal by fluorescence. The focused dc laser delivered about 600 mW, and the fluorescence lifetime of the excited state of NO_3 is 30–300 μs.[5] Under these conditions, resonance Raman emission could be competitive with spontaneous emission, and both could be observed together. The spike would then necessarily move around with the exciting laser line, as observed (Figs. 7–9). Upon excitation into vibrational states of the upper electronic state (Figs. 11–13), no spikes originate from vibrationally deactivated molecules, and all cases of observed spikes originate at the energy level populated by the exciting frequency.

The vibrational bands typically have FWHM of about 60 to 110 cm^{-1}, and under our resolution the spikes have FWHM of about 5 cm^{-1}. The presence of the spikes as sharp markers gives better estimates of the energy-level separations than would be possible with spike-free peaks.

The sharp spike does not appear on the bands that peak at 368, 1923, and 2155 cm^{-1} (Figs. 4 and 6), and no spikes appear on any band excited from the hot band at 368 cm^{-1} (Fig. 14). There seems to be no simple explanation for this lack of resonance Raman line on these bands. However, some observed spikes are extremely weak and almost not seen in Figs. 7(A), 7(B), 8(B), and 9(A), and the blunt peak at 693 cm^{-1} in Figs. 8(A) and 8(B) moves with excitation line inside the 0–0 band like a spike. The failure to observe a spike on the ν_4 and other bands may be due to quantitative features, such as differences in overlap integrals.

D. Qualitative resolution of the C_{2v} and D_{3h} aspects

Experiments. The infrared spectra of NO_3 (Refs. 6–8) prove that there is D_{3h} symmetry with respect to the rotational structure of two vibrational bands. Analysis of our observed fluorescence frequencies suggests the need for a fifth fundamental vibrational frequency, which is inconsistent with strict, unperturbed D_{3h} symmetry.

Theory. Table I and references there show that molecular structure theorists have long-standing disagreement as to whether NO_3 has C_{2v} or D_{3h} symmetry.

Qualitative resolution. The potential-energy surface (Fig. 1), vibrational analysis of Cu_3 by Morse *et al.*,[19] and the theoretical study of Stanton, Gauss and Bartlett[18] provide a possible explanation to resolve this apparent conflict. As suggested by Kawaguchi *et al.*,[8] there are shallow potential wells that tend to make one NO bond in NO_3 slightly longer than the other two bonds with low barriers between the three equivalent C_{2v} minima. Davy and Schaefer[14] found the energy difference between the D_{3h} minimum and C_{2v} minima to be 490 cm^{-1}. Stanton, Gauss, and Bartlett found C_{2v} well depth of about 900 cm^{-1} and the barriers between the three C_{2v} minima of about 190 cm^{-1} (possibly comparable or even larger errors are pointed out by the authors). The vibrational frequencies of 1053, 1500, and 2010 probably have zero-point energies greater than the barrier height between the three equivalent miniwells. The out-of-plane bending mode at 753 cm^{-1} is not included in the PES of Fig. 1. The mode at 368 cm^{-1} has zero-point energy comparable to the height of the barrier separating the three miniwells.

The vibrational coordinates and frequencies as derived by Morse *et al.*[19] for Cu_3 show rather normal symmetric stretching motion, but the antisymmetric motions are strongly perturbed and unusual. The antisymmetric stretching mode shows "pseudorotation," that is, the stretched corner of the triangle permutes as if a rotation around the three positions. The D_{3h} degeneracy is split on the time scale of this vibrational motion.

Following Stanton, Gauss, and Bartlett, we propose a similar explanation for NO_3. On the time scale of molecular rotations, vibrational modes average to give D_{3h} structure and rotational spectra, in agreement with Refs. 6–8. On the time scale of molecular vibrations there are interactions that split the degeneracy of the modes normally associated with a D_{3h} molecule.

ACKNOWLEDGMENTS

This work was supported by the Director, Office of Energy Research, Office of Basic Energy Sciences, Chemical Sciences Division of the U.S. Department of Energy under Contract No. De-AC03-76SF00098. The support from Dr. R. Davy, Dr. K. Kawaguchi, H. F. Schaefer, and A. Weaver in sharing important information about their research results is greatly appreciated. We are grateful to Professor E. Hirota for very helpful discussions.

[1] D. A. Ramsay, Proc. Colloq. Spectrosc. Int. **10**, 583 (1962).
[2] W. J. Marinelli, D. M. Swanson, and H. S. Johnston, J. Chem. Phys. **76**, 2864 (1982).
[3] A. E. Douglas, J. Chem. Phys. **45**, 1007 (1966).
[4] T. Ishiwata, I. Fugiwara, Y. Naruge, K. Obi, and I. Tanaka, J. Phys. Chem. **87**, 1349 (1983).
[5] H. H. Nelson, L. Pasternack, and J. R. McDonald, J. Phys. Chem. **87**, 1286 (1983); J. Chem. Phys. **79**, 4279 (1983).
[6] T. Ishiwata, I. Tanaka, K. Kawaguchi, and E. Hirota, J. Chem. Phys. **82**, 2196 (1985).
[7] R. R. Friedl and S. P. Sander, J. Phys. Chem. **91**, 2721 (1987).
[8] K. Kawaguchi, E. Hirota, T. Ishiwata, and I. Tanaka, J. Chem. Phys. **93**, 951 (1990).
[9] A. Weaver, D. W. Arnold, S. E. Bradforth, and D. M. Neumark, J. Chem. Phys. **94**, 1740 (1991).
[10] A. Lund and K. Thuomas, Chem. Phys. Lett. **44**, 569 (1976).
[11] P. E. M. Siegbahn, J. Comput. Chem. **6**, 182 (1985).
[12] U. Kaldor, Chem. Phys. Lett. **166**, 599 (1990).
[13] R. C. Boehm and L. L. Lohr, J. Phys. Chem. **93**, 3430 (1989).
[14] R. D. Davy and H. F. Schaefer III, J. Chem. Phys. **91**, 4410 (1989).
[15] B. Kim, B. L. Hammond, W. A. Lester, Jr., and H. S. Johnston, Chem. Phys. Lett. **168**, 131 (1990).
[16] R. D. Davy (private communication).
[17] V. R. Morris, S. C. Bhatia, and J. H. Hall, J. Phys. Chem. **94**, 7414 (1990).
[18] J. F. Stanton, Juergen Gauss, and Rodney J. Bartlett, J. Chem. Phys. **94**, 4084 (1991).
[19] M. D. Morse, J. B. Hopkins, P. R. R. Langridge-Smith, and R. E. Smalley, J. Chem. Phys. **79**, 5316 (1983).
[20] J. P. Devlin and I. C. Hisatsune, Spectrochim. Acta **17**, 206 (1961).
[21] D. L. Bernitt, R. H. Miller, and I. C. Hisatsune, Spectrochim. Acta **23A**, 237 (1967).
[22] T. Tanaka and Y. Morino, J. Mol. Spectrosc. **32**, 430 (1969).
[23] R. A. Graham and H. S. Johnston, J. Phys. Chem. **82**, 254 (1978).